Analysis of VE/TR salt cavern cluster leakage incident of 20 April 2018

October 16th, 2018

Analysis of VE/TR salt cavern cluster leakage incident of 20 April 2018

Author:

Prepared for:
Nedmag
T.a.v.
Bilitonweg 1
9640 VE Veendam

Prepared by:
PanTerra Geoconsultants B.V.
Weversbaan 1-3
2352 BZ Leiderdorp
The Netherlands
T +31 (0)71 581 35 05
F +31 (0)71 301 08 02
info@panterra.nl

Contents

Summary

An analysis was carried out of the leakage incident on 20 April 2018 when, most probably as a result of a leak in the Halite roof, significant volumes of brine escaped at high rate into the overburden above the Halite. The analysis was carried out using two different hydraulic fracture propagation simulators, that can be considered as complementing each other.

The simulation results show that as a result of initial high-rate flow immediately following the incident, a large hydraulic fracture was created. This fracture likely propagated upwards into overburden formations up to the Vlieland sands / clays and the overlying chalk. It possibly propagated even further upward into the shallow high-permeability sands (Drenthe, Peelo, Peize, Waalre, Oosterhout), depending primarily on the magnitude of (possible) in-situ stress contrasts between the Vlieland sands and clays, and on the permeability of the Vlieland sands.

The simulation results also show that this hydraulic fracture reached its maximum upward extent right in the beginning during the period of high injection rate. The results did not indicate further upward fracture growth during the subsequent periods of medium/low rate injection rate. This is in line with general understanding of such fractures, which are primarily driven by (lack of) leak-off into the formations around them.

The fracture simulations show that below the high-permeability shallow sands, most leak-off takes place into the Vlieland sandstone at about 1100 m depth. From geological analysis it is known that the Vlieland is a laterally continuous sandstone layer with no flow baffles over the Veendam pillow. A pressure transient analysis was carried out which demonstrated that charging of this formation by brine from the leakage incident plus subsequent continuous low-rate injection is not expected to result in laterally extensive areas of high pore pressure.

Epilogue October 2018

The fracture propagation study reported in this memo was carried out during May and June 2018, during a period that low-rate leakage was still ongoing. Meanwhile, based on the behaviour of the cavern cluster and on subsidence measurements, it was concluded that the leakage came to a halt significantly quicker than assumed initially. Volume balance calculations and pressure transient analysis using these latest results indicate that final pore pressure penetration into the Vlieland sandstone before the leakage stopped has been very limited.

1. Introduction

On 20 April 2018, the Halite roof above the Carnalite formation that is being used for salt mining started leaking. This resulted in a rapid annulus pressure drop in a number of interconnected solution mining wells operated by Nedmag west of Veendam. It appeared that this event resulted in brine injection into the overburden at high initial rates (order 50.000 m^3/h). This rate declined fairly quickly into 'moderate' rates (around 1000 m^3/hr) which after two days had dropped further down to about an assumed 100 m^3/hr. Current rates are of the order 50 m^3/hr as a result of continuing cavern cluster convergence. It is estimated that within the first month following 20 April, about 150.000 m^3 of brine leaked away into the overburden.

This study was conducted to analyse the leakage event and the subsequent month, in particular to assess the risk of hydraulic fracture (non-)containment to the subsurface during the event itself and thereafter, and to assess the risk of (high) pressure charging of extensive areas in the subsurface.

Panterra carried out a simulation study of hydraulic fracture propagation as a result of the leakage incident in the overburden layers above the Halite. Also a pressure transient analysis study was carried out to assess the lateral extent of high pressure areas because of brine leakage in overburden formations nonzero permeability.

In order to assess uncertainties in the overburden formations above the Halite, a number of relevant parameter sensitivities was investigated.

This memo is organised as follows. Paragraphs 2 and 3 introduce the used methodologies in more detail, and discuss the input parameters for the base case subsurface model (geology, etc.). Paragraphs 4 and 5 present and discuss the main results of the base case and sensitivity studies. Conclusions are listed in paragraph 6. Finally, paragraph 7 is an epilogue to the original fracture propagation study in which the latest insights based on more recent measurements are presented.

2. Methodologies

2.1 Simulation of hydraulic fracture propagation

The primary model that was used in this study is one that was developed for simulation of hydraulic fractures resulting from water injection (WI) (e.g. waterflooding, water injection disposal), cuttings re-injection (CRI) and hydraulic fracture (HF) stimulation [1-4] ('WI/CRI fracture model'). This model was extensively applied in the field [e.g. 5-20] and also validated against other models and against field data (see Appendix B for a more detailed overview of the validations). The pro's and con's of using this model are listed below:

- PLUS: Leak-off / flow in the reservoir is properly modeled
- PLUS: Numerical stability, works well in connection with 3D reservoir simulator
- MINUS: The model uses an assumed fracture shape (two half-ellipses)

Because of the last 'con' (model uses an assumed fracture shape), also a number of simulations was carried out using a so-called 'boundary element model' ('BEM fracture model') in which the hydraulic fracture is subdivided in a grid. This is a commercial model that was developed for predictions and designs of pump (proppant) schedules in hydraulic fracture stimulation and for predictions in cuttings re-injection [21]. The pro's and con's of using this model are listed below:

- PLUS: Good (more detailed) description of the shape of the fracture (because of the gridding) and its evolution during injection. Therefore better in modelling the details of fracture geometry (horizontal, vertical) per layer.
- MINUS: Program has been built for modelling hydraulic fracture stimulation and cuttings re-injection, where leak-off rates are relatively low. Therefore, it is unsuited for modelling situations with (relatively) high leak-off, such as most cases of water injection.
- MINUS: The physical process of fracture propagation is extremely difficult to describe on a grid, and therefore such simulation programs are often numerically fairly unstable.

2.2 Pressure transient calculations of pore pressure penetration

A number of the overburden formations has nonzero permeabilities (for further details see below), and it is likely that over time brine will leak away into those formations, thus resulting in high-pressure areas in those formations around the hydraulic fracture. The development of these high-pressure areas was computed using analytical solutions to the diffusivity equation for two types of geometries: linear (perpendicular to the fracture) and elliptical. In the latter case a methodology was used as developed earlier for pressure transient analysis around fractured injection wells [22].

3. Input data (see appendix A for details)

3.1 Geology

Geology of the overburden layers above the Halite was based on the TNO database DinoLoket. A simplified geological model (as used in the simulations) is shown in figure 1 below.

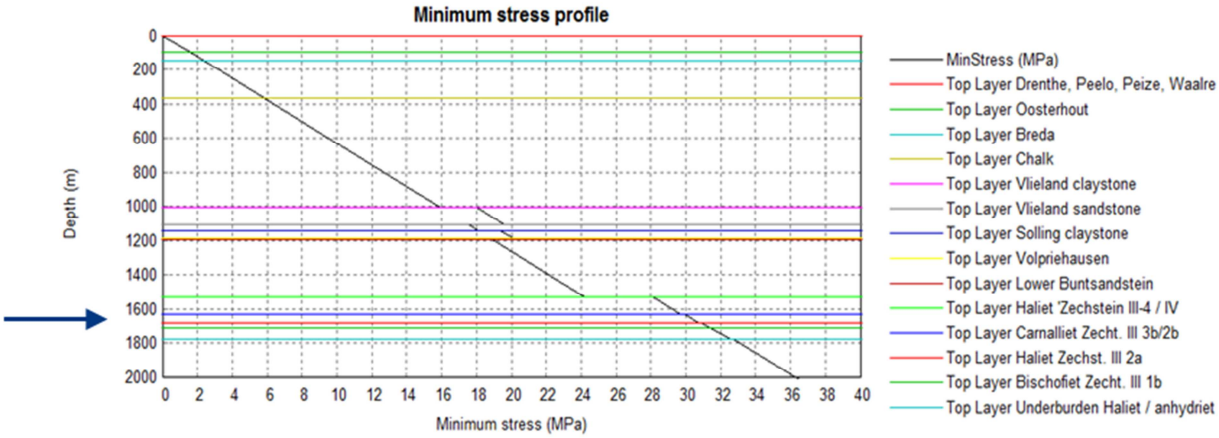

Figure 1. Simplified 'layer-cake' geology of the salt layers plus overburden layers

The minimum principal in-situ stress gradient in this figure is given by the typical value of 0.158 bar/m for a tectonically quiet stress regime [23]. The salt layers have a higher gradient of about 0.18 bar/m which represents the relaxed salt stress state due to mining, based on the pressure stabilisation of the cavern after the first 2 weeks. In figure 1 this is exhibited by the stress 'jump' when moving down from the lower Buntsandstein into the Halite (Zechstein III-4 / IV).

Details of the in-situ stress profile within the overburden are unknown. Based on geology (sands versus clays), and using Eaton's rule with different values for Poisson's ratio, a 'base case' in-situ stress profile was computed. However, because of the inherently large uncertainties, sensitivities were carried out in which the stress contrasts between sands and clays were varied.

3.2 Layer properties

Young's moduli were estimated using typical 'ballpark' figures. The salts are known to be very stiff with a high Youngs'modulus in the order of 25 GPa.

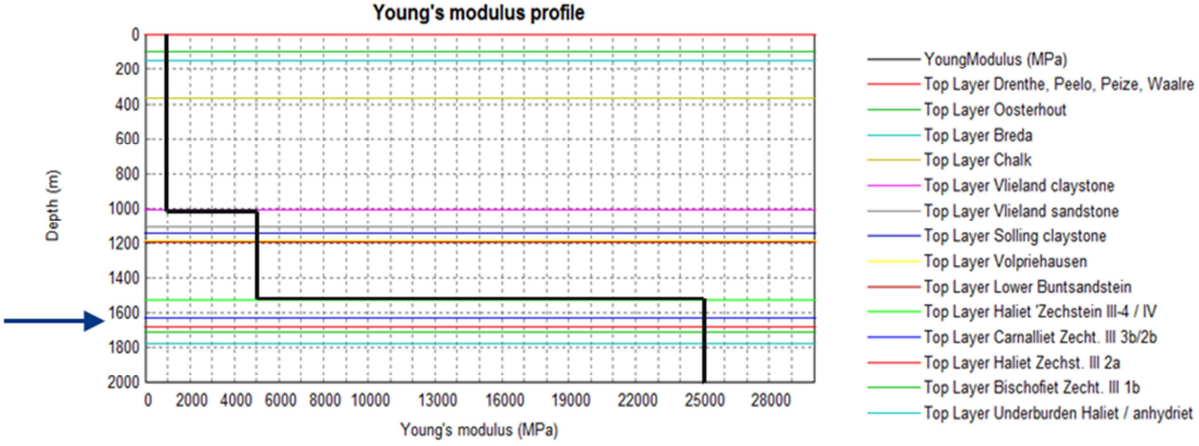

Figure 2. Young's modulus profile

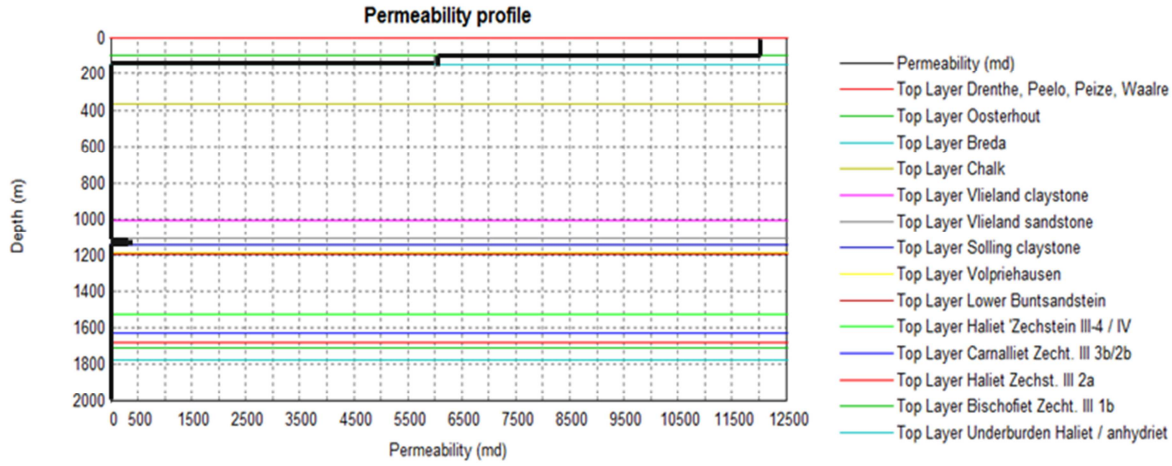

Figure 3. Permeability profile

The intermediate layers (lower Buntsandstein up to Vlieland claystone) are medium stifness rocks, and they were assigned a value of Young's modulus equal to 5 GPa. Finally, the top layers (chalk and upwards) were assigned values of Young's modulus typical for weakly consolidated sandstone: 1 GPa. This value may be on the high end for the top high-permeability unconsolidated sands (Drenthe, Peelo, Peize, Waalre, Oosterhout), so sensitivities were run in which the Young's moduli for these sands are equal to 0.1 GPa.
Figure 3 shows the permeability profile. As can be seen, except for the unconsolidated sands at the top, overburden permeabilities are generally low, with the highest values occurring in the 35 m thick Vlieland sandstone.

3.3 Other input parameters

Within the WI/CRI hydraulic fracture simulation model, leakage around the injector is modelled using a simple reservoir in late-time transient flow, where the zones of different mobility around the injector and the drainage radius are assumed to have an elliptical shape [3,4]. Zones of different mobility around the injector are generally the result of temperature (cold versus warm water) and difference between injection and reservoir fluids (e.g. water versus oil). In order to capture this in the simulations, the model requires input covering viscosities, relative permeabilities, and drainage radius.

Poroelastic and thermoelastic constants and reservoir temperature are required to compute poroelastic and thermoelastic stresses around the injector. Thermoelastic stresses are a result of (often cold) water leakage into the reservoir. This is typically of importance for cases where large volumes are injected into formations with medium to high permeability. However, since in the present study the permeabilities of most of the formation layers were low down to (almost) zero, the poroelastic constant and thermoelastic constant were set equal to zero.

The injected brine is 'clean' in the sense that it does not contain solid contaminants that can plug the formation pores and thus form an external filtercake on the fracture face.

The leakage incident and the first month thereafter were modelled in this study by three subsequent injection cycles:

1. Very high rate (50000 m^3/h) during 30 minutes
2. High rate (1050 m^3/h) during 47,5 hours
3. 'Medium' rate (100 m^3/h) during 30 days

The above three cycles are an approximation of a long continuous leakage at decreasing rates. The 100 m^3/h of the last cycle is the high end leakage rate, based on high end cavern convergence rates, with deduction of the (net) produced brine volumes.

4. Results for base case (see also Appendix C)

4.1 Fracture simulations: WI/CRI model

Results of fracture simulations using the WI/CRI model are shown in figures 4 a,b,c.

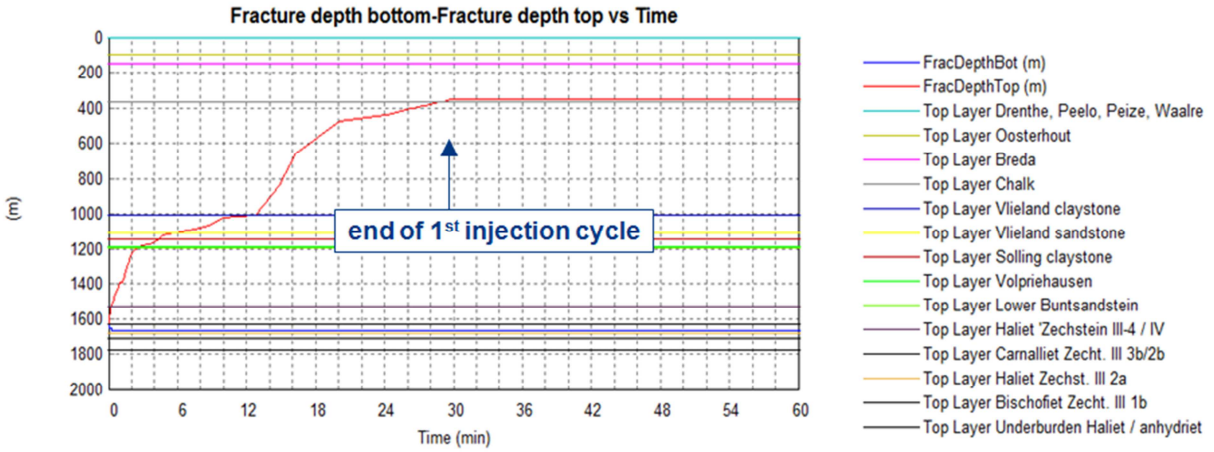

Figure 4a. Results after one hour of injection of simulations using WI/CRI model

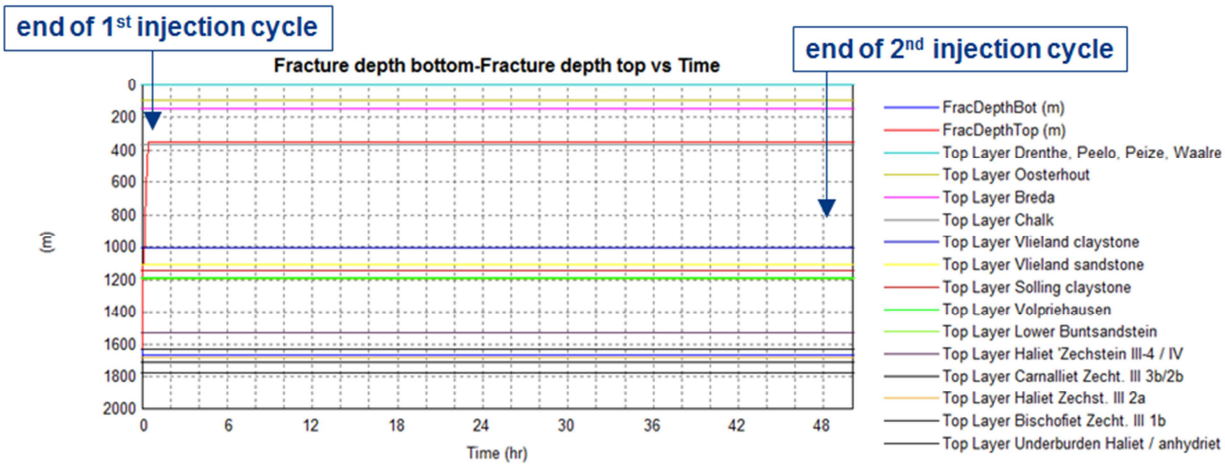

Figure 4b. Results after two days of injection of simulations using WI/CRI model

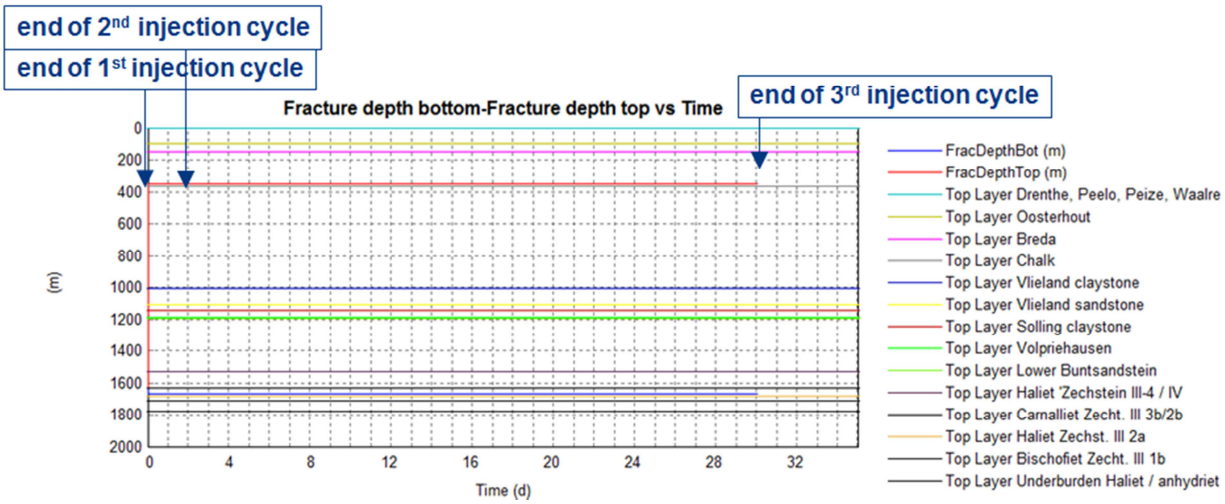

Figure 4c. Results after one month of injection of simulations using WI/CRI model

The corresponding simulated 'wellhead' injection pressures are shown in figures 5 a,b,c.

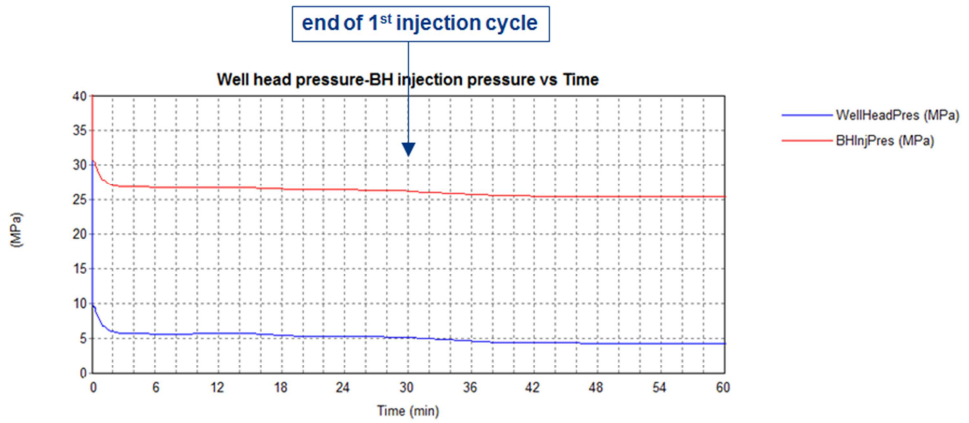

Figure 5a. Computed injection pressures after one hour of injection by simulations using WI/CRI model

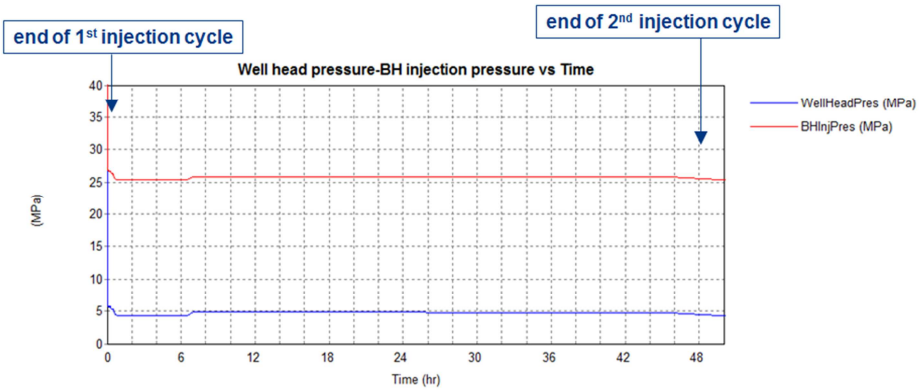

Figure 5b. Computed injection pressures after two days of injection by simulations using WI/CRI model

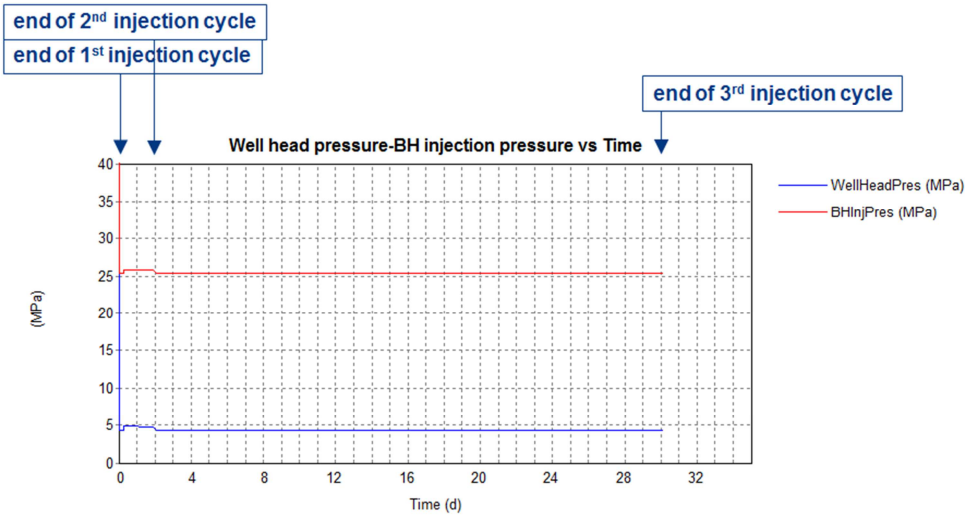

Figure 5c. Computed injection pressures after one month of injection by simulations using WI/CRI model

Discussion Based on the results shown in figures 4 and 5, the following points are noted:

- During the first (high-rate) injection cycle of 30 minutes, a fracture is created which grows upwards to about 350 m depth in the Breda formation (fig. 4).

- During the second cycle, injection rate is much lower. Because the fractures are leak-off driven it is possible that the injection pressure drops below the fracture closure pressure leading to partial fracture closure, i.e. fracture shrinkage. This is in line with general experience from waterflooding operations.
- In this case, one can see that lowering the injection rate in the 2nd injection cycle is predicted to result in only a modest drop in injection pressure (± 1 MPa) for a stationary fracture (fig. 5).
- Therefore, the injection pressure does not appear to drop below the closure pressure and the fracture likely stays open over its entire length and height.
- Unfortunately, the WI/CRI model cannot handle shrinking fractures, only stationary and growing fractures. This means that (partial) fracture closure (shrinkage) is not visible in the results of the WI/CRI model.
- Because of the above shortcoming, in the modelling study it was assumed that the hydraulic fractures did not (partially) close (shrink) as a result of lowering injection rate. This approach can be considered conservative from the viewpoint of estimating the risk of (significant) upward fracture growth as a result of the leakage incident.
- During the 2nd injection cycle, the injection pressure is seen to rise slightly over time, but not beyond the propagation pressure (fig. 5).
- In the 3rd cycle, the injection pressure again shows a modest drop (fig. 5)
- In the 2nd and 3rd injection cycles, the fracture does **not** grow beyond its size resulting from the 1st injection cycle (fig. 4). This is in line with what one expects for such leak-off driven fractures.

4.2 Fracture simulations: Boundary element model (BEM)

Results of fracture simulations using the BEM fracture model are shown in figures 6 a and b.

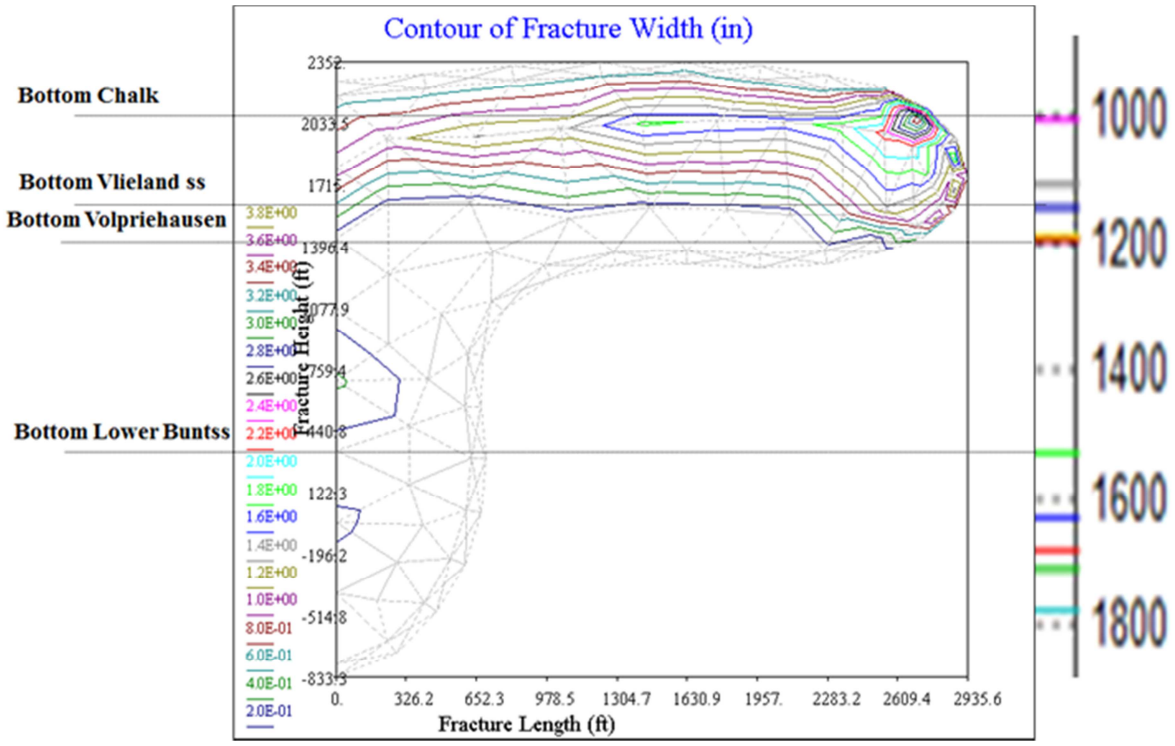

Figure 6a. Fracture geometry (plus mesh) after 30 minutes of injection, simulations using BEM model

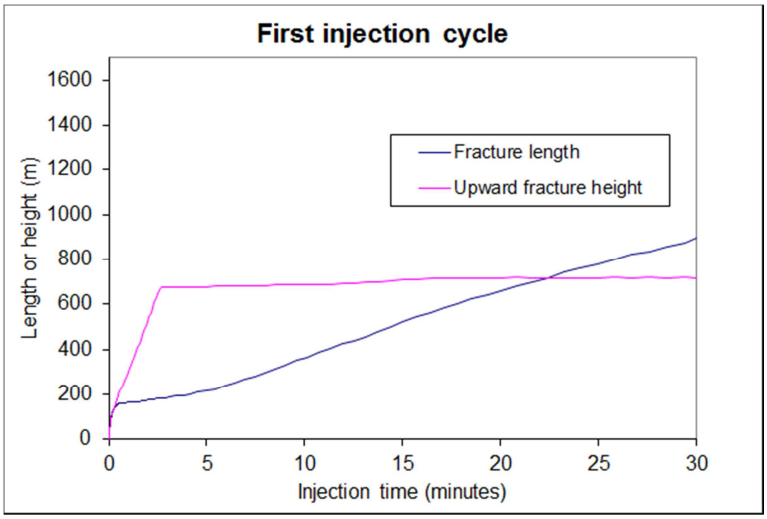

Figure 6b. Fracture growth during first 30 minutes of injection, simulations using BEM model

Discussion Based on the results shown in figure 6, the following points are noted:

- With the BEM model, it proved to be only possible to simulate the high-rate first injection cycle (50000 m^3/h during 30 minutes). Attempts to simulate the subsequent cycles were unsuccessful because of excessive leak-off rate as compared to injection rate (for which this program was not built), which resulted in crash of the program.
- The fracture grows up to +/- 900 m depth (100 m into the Chalk) which is +/- 500 m deeper than predicted by the other (WI/CRI) model. As will be shown as part of the sensitivity study below, this is largely due to the presence of an appreciable (± 20 bar) stress contrast between Vlieland sandstone and Vlieland clay. This stress contrast is responsible for significantly limiting upward fracture growth in the predictions by the BEM model, contrary to the predictions of the WI/CRI model (fig. 4) in which the impact of this (20 bar) stress contrast is limited.

4.3 Pore pressure penetration

Results of pore pressure penetration calculations for the Vlieland sandstone and the Bunter are shown in figures 7 and 8 below. These pore pressure penetration calculations assume a **constant pressure** (not rate) boundary condition at the location of the well. The values for these pressures (66 bar in the Vlieland and 80 bar in the Bunter) are based on the initial bottom-hole injection pressure in TR-2 corrected for the hydrostatic gradient of the brine. The assumption of constant pressure at the wellbore is conservative because observations show that this pressure has been (in still is) slowly declining over time.

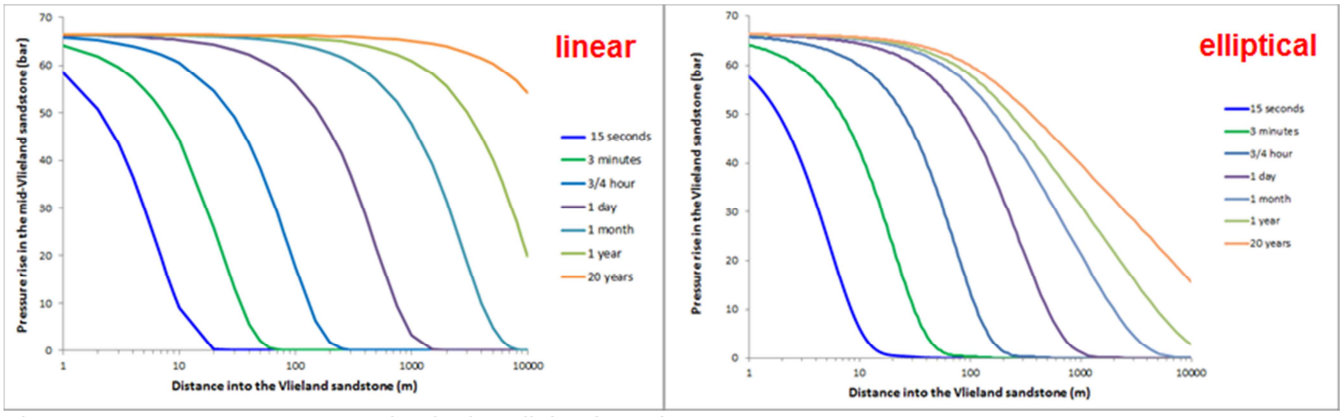

Figure 7. Pore pressure penetration in the Vlieland sandstone

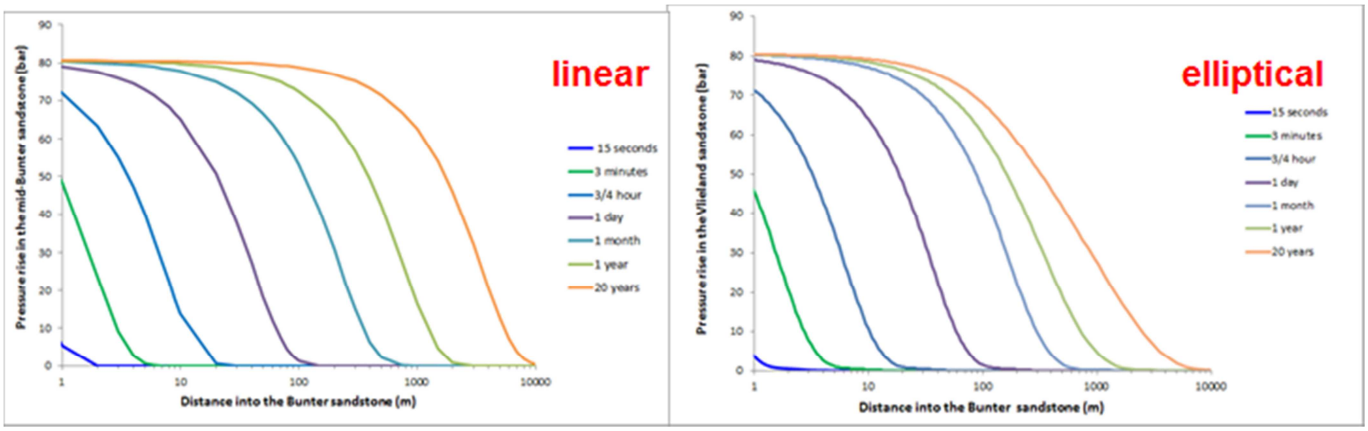

Figure 8. Pore pressure penetration in the Bunter sandstone

The linear pore pressure penetration fronts are the most conservative ones, because they assume pore pressure penetration taking place in only one dimension (i.e. perpendicular to the fracture face). However, in reality when the pressure penetration front becomes of the same size as the fracture length, pore pressure will further penetrate the formation in a 2D elliptical way. This is corroborated by figures 7 and 8, where one can see that for short times, the linear and elliptical fronts coincide, but for longer times, the elliptical fronts move more slowly.
Overall, one can conclude that in the Vlieland sandstone, pore pressure will have penetrated by about 50% at 1 km from the injector after one year. In the Bunter sandstone, penetration is significantly slower, entirely in line with expectations.

4.4 Cumulative brine volumes leaked away

See the tables below for estimates. These tables are based on the following assumptions about injection rates:

- First month: 50000 m^3/h for 30 minutes, followed by 1050 m^3/h for 47.5 hours, followed by 100 m^3/h for 30 days.
- Second month and thereafter: 50 m^3/h.

Formation	Brine volume leaked away (m^3)	Brine penetration front (m)
Chalk	5600	0,54
Vlieland sandstone	132000	39
Volpriehausen	4400	6,7
Lower Bunter	4300	0,27
TOTAL in first month	~146000	
Total in a year assuming a constant rate of 50 m^3/hr	~ 438000	

Injection duration	Brine penetration front into Vlieland sandstone (m)
1 month	39
1 year	110
2 years	176
3 years	220
5 years	290
10 years	417
20 years	595

- In total, about 146000 m^3 has leaked away during the first month
- In total, about 438000 m^3 leaks away per year, assuming a constant leakage rate of about 50 m^3/hr (in the first year, about 550000 m^3 leaks away).
- The highest volumes (about 90% of total) leak into the Vlieland sandstone
- PLEASE NOTE: The pressure penetration front is far ahead of the brine penetration front!

5. Sensitivities (see also Appendix C)

5.1 Overview of sensitivities

An overview of all sensitivities that were carried out is given in the table below. The following paragraphs will focus on the most important sensitivities (i.e. the ones that yielded significantly different results from the base case) which have been indicated in blue in the table below. For results of the other sensitivities, the reader is referred to Appendix C.

No	Description of sensitivity	Possibly in combination with ….			
		a	b	c	d
1	No stress contrasts between sands and clays	Low E (0.1 GPa) in top sands (Drenthe, Peelo, Peize, Waalre, Oosterhout)	No stress contrasts only between Vlieland sands and clays	Low stress contrasts only between Vlieland sands and clays	High stress contrasts only between Vlieland sands and clays
2	Injection point in top Halite				
3	Low $k_{Vlieland}$ (30 mD)				
4	High $k_{Vlieland}$ (3000 mD)				
5	High injection rates	Low E (0.1 GPa) in top sands	High injection rate first cycle (BEM)		
6	Low injection rates				
7	Low k_{Bunter} (0.1 mD)				
8	High k_{Bunter} (10 mD)				
9	All k divided by 3				
10	All k multiplied by 3				
11	Initial fracture length 100 m				
12	Initial fracture length 50 m				

5.2 Stress contrasts (sensitivities no 1, 1b and 1c)

This sensitivity focuses on the question of how the stress contrasts between sands and clays in the overburden affect the degree of upward fracture growth. Fig 9 below shows the case of zero stress contrasts between sands and clays.

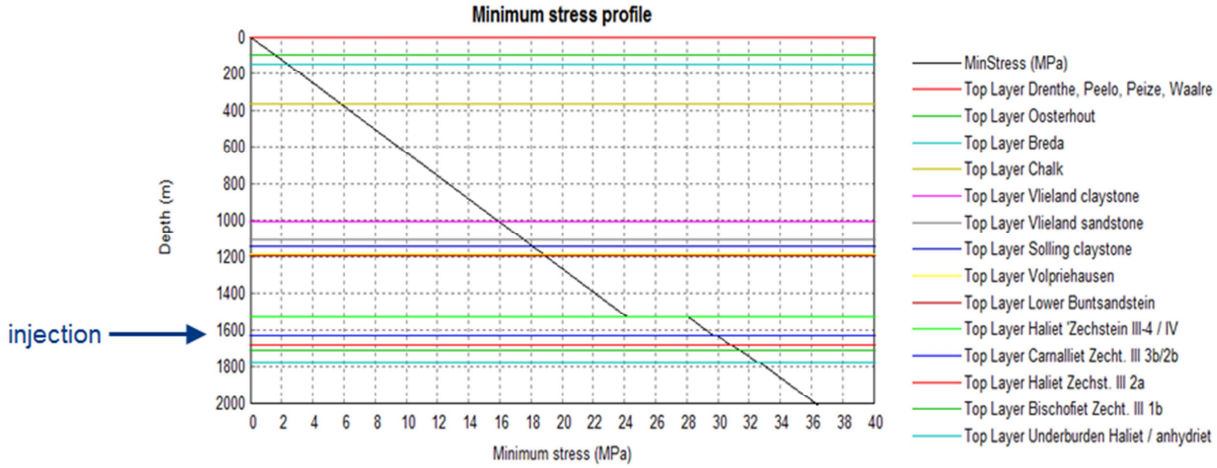

Figure 9. Zero stress contrasts between sands and clays in the overburden

As was menioned before (see discussion around figure 6), hydraulic fracture growth as computed by the BEM model was strongly influenced by the presence of stress contrasts between sands and clays. Therefore, the following discussion focuses on this model.

Results computed by the BEM model in the absence of stress contrasts are shown in fig. 10.

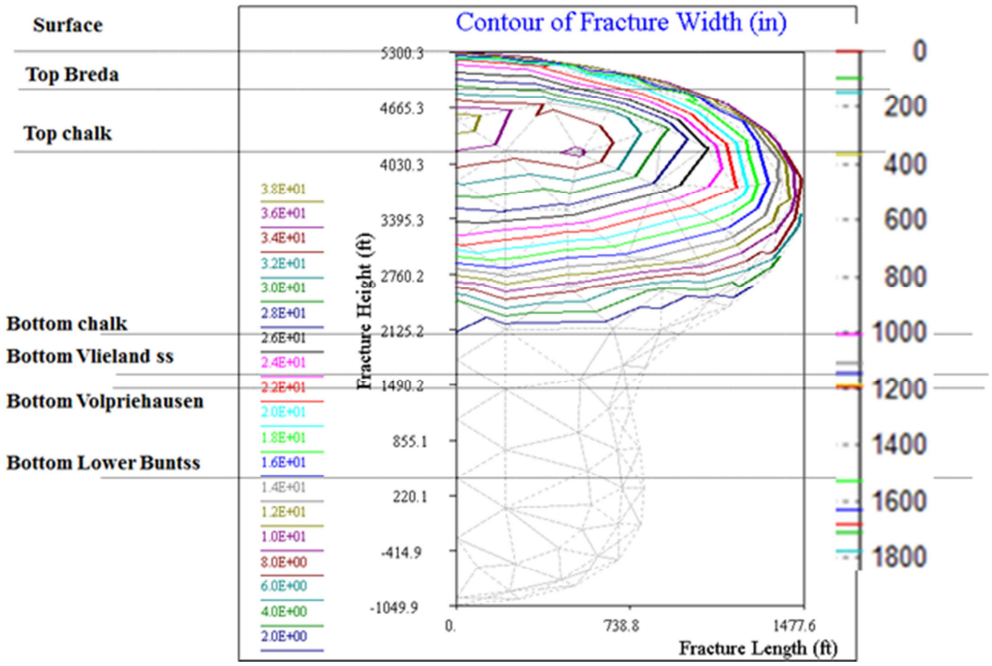

Figure 10a. Fracture geometry (plus mesh) after 28 minutes of injection, simulations using BEM model, no stress contrasts between sands and clays.

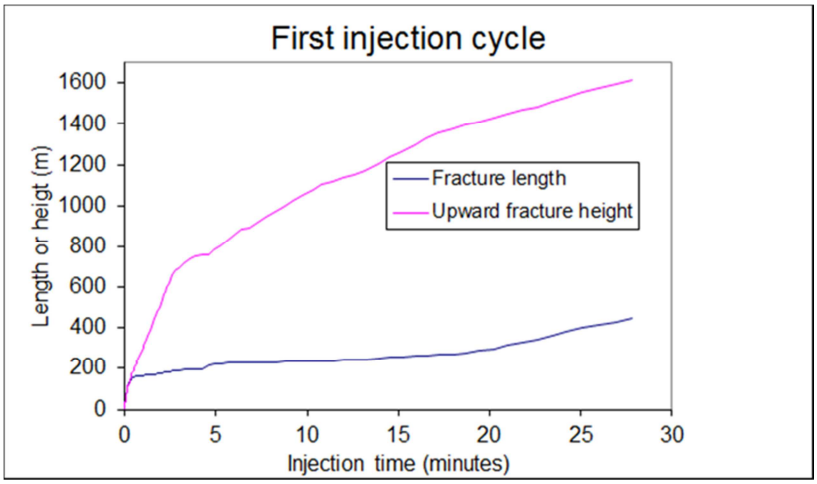

Figure 10b. Fracture growth during first 28 minutes of injection, simulations using BEM model, no stress contrasts between sands and clays.

From figure 10, it can be seen that the fracture reaches surface after 28 minutes of injection despite the shallow high-permeability sands. Thus, it is clear that there is a very strong sensitivity to the presence of stress contrasts. Further exploring this sensitivity, it was found that it is primarily the stress contrasts between the **Vlieland** sands and clays that impact upward fracture growth. This was demonstrated by a sensitivity in which **only** the stress contrasts between the Vlieland sands and Vlieland clays was removed. The result was very similar to Fig. 10, with the only difference that after 30 minutes of injection, the fracture had grown upward into the shallow sands up to ~ 200 m below surface (sensitivity 1b).

What happens when a **low** stress contrast between the Vlieland sands and clays is introduced? This is shown below, where the stress contrast between the Vlieland sands and clays was lowered from 20 bar (base case) to 10 bar.

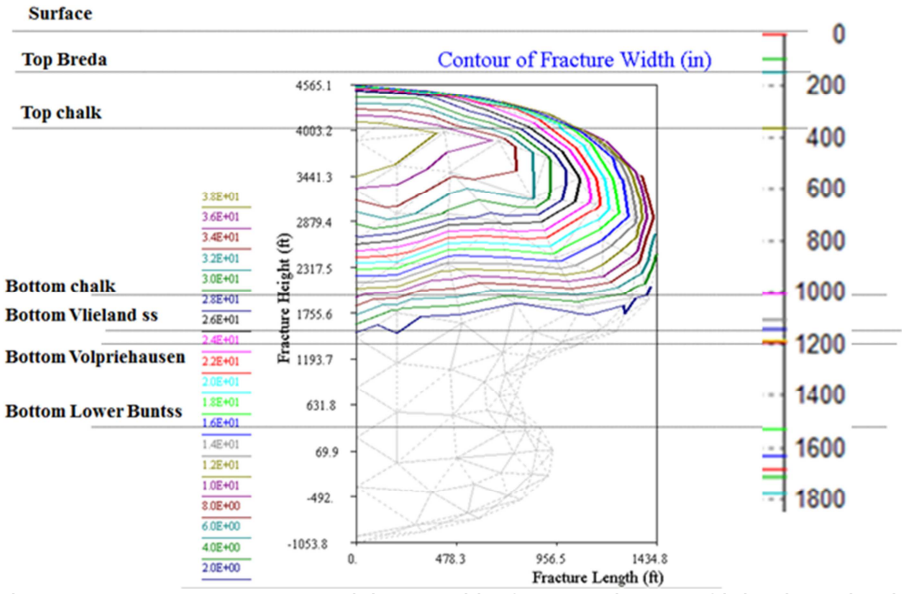

Figure 11. Fracture geometry (plus mesh) after 30 minutes of injection, simulations using BEM model, low stress contrasts between Vlieland sands and clays

Figure 11 shows that for stress contrasts with a magnitude equal to 50% of the base case, the fracture is hardly stopped in the deeper layers and grows more or less unhindered to the shallow sands (although upward growth is somewhat retarded with respect to the situation in figure 10), entirely in line with expectations.

Finally, figure 12 shows the results of simulations using the WI/CRI model without stress contrasts. As can be seen, there are only minor differences with figure 4 (base case).

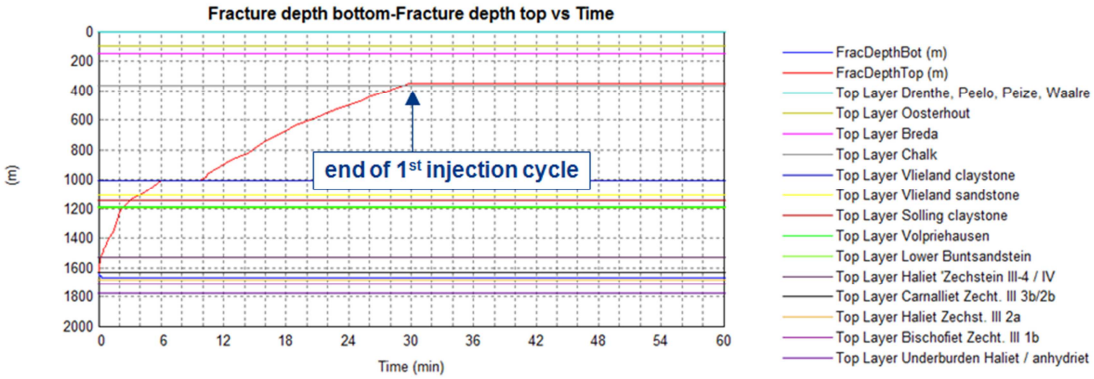

Figure 12. Results after one hour of injection of simulations using WI/CRI model. No stress contrasts between sands and clays.

5.3 Injection rate (sensitivities no 5 and 6)

In the sensitivity of high injection rate, the base case injection rates of all three cycles were multiplied by 1.5, resulting in the following rates per cycle: 75000 m^3/h, 1575 m^3/h, and 150 m^3/h. Results for the WI/CRI model are shown in fig 13 below.

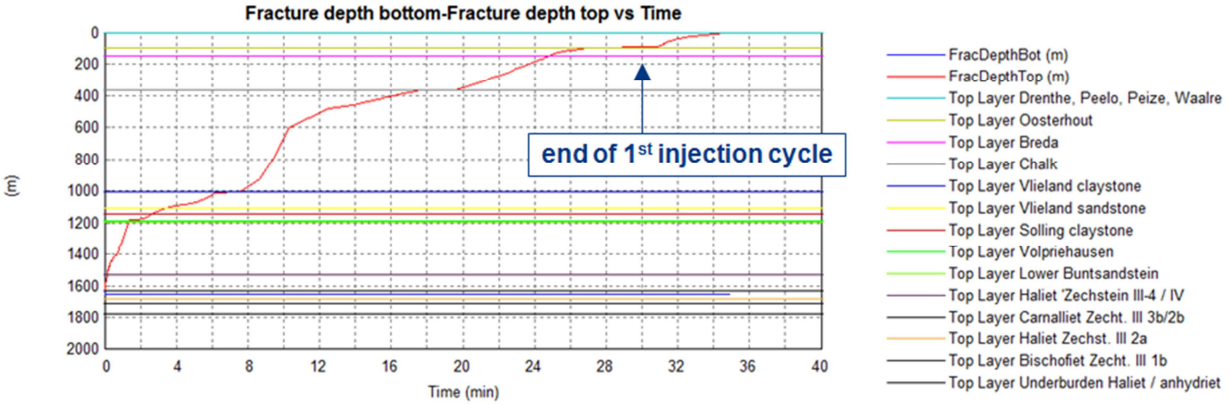

Figure 13. Results after 40 minutes of injection of simulations using WI/CRI model. High injection rates.

Figure 13 shows that after about 40 minutes, the fracture reaches the surface. Also the BEM model results in a larger hydraulic fracture (see appendix C). Figure 13 is of course not surprising, and is further corroborated by fig. 14 which shows the results for 'low' injection rates (25000 m^3/h – 525 m^3/h – 50 m^3/h). In the latter figure, is can be seen that the resulting hydraulic fracture is significantly smaller than in the base case.

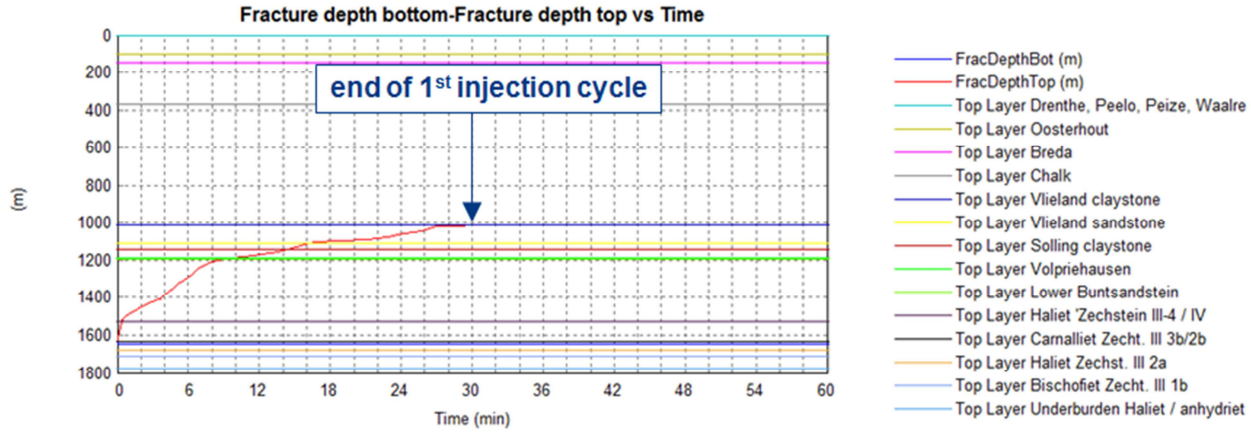

Figure 14. Results after 60 minutes of injection of simulations using WI/CRI model. Low injection rates.

5.4 Low Young's modulus of top sands (sensitivities 1a and 5a)

Results are shown in figures 15 and 16 below for two different situations.

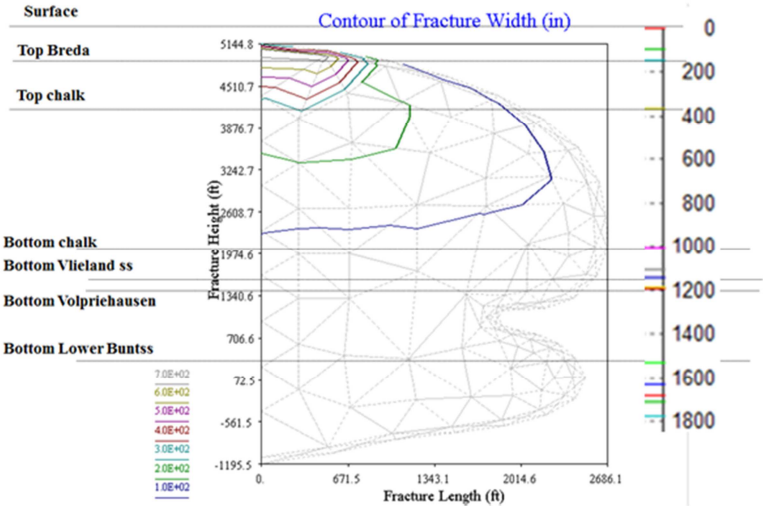

Figure 15. Fracture geometry (plus mesh) after 30 minutes of injection, simulations using BEM model, no stress contrasts between sands and clays, low modulus in top sands (0.1 GPa).

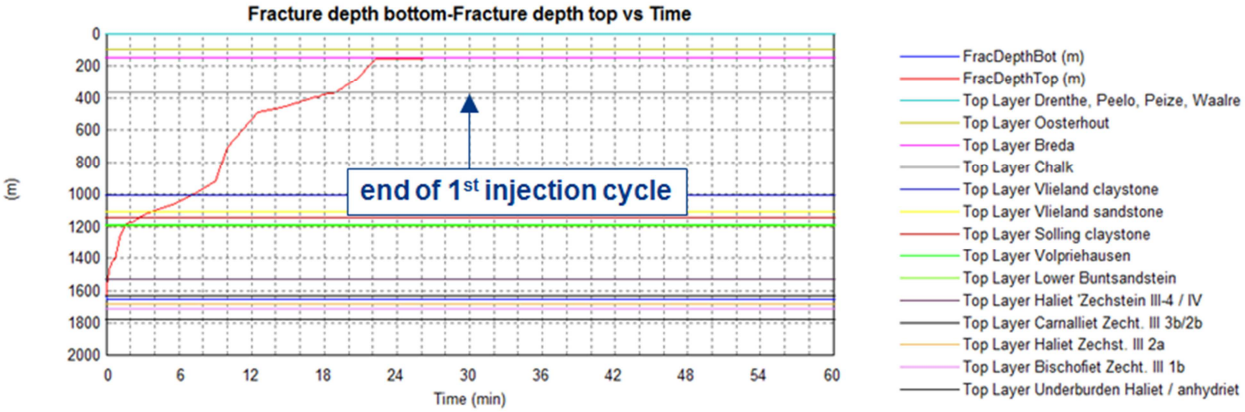

Figure 16. Results after 1 hour of injection of simulations using WI/CRI model. High injection rates, low modulus in top sands (0.1 GPa).

When the results of figures 15 and 16 are compared to figures 10a and 13, respectively, it can be seen that the fracture no longer grows to surface. This is in line with expectations, because a lower Young's modulus (0.1 GPa) for the shallow high permeability sands helps to retard upward fracture growth because larger deformations are allowed before the formation starts to crack.

5.5 Low permeabilities of sandstones

First, only the sensitivity of a low permeability for the Vlieland sandstone was investigated (sensitivity 3). For this sensitivity, the permeability of the Vlieland sandstone had to be lowered by a factor 10 (i.e. to 30 mD) in order to observe a clear difference with the base case. Results are shown in figures 17a and b below.

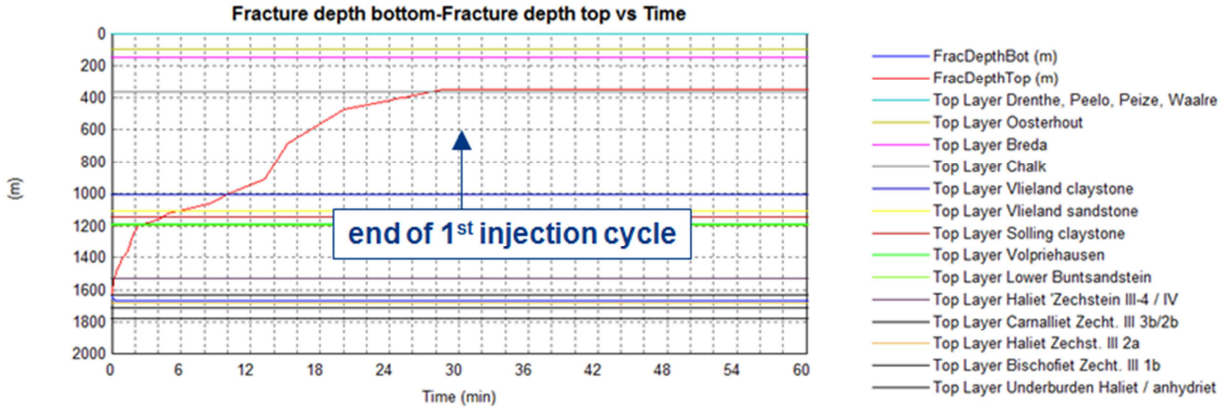

Figure 17a. Results after 60 minutes of injection of simulations using WI/CRI model. Low permeability of Vlieland sandstone (30 mD).

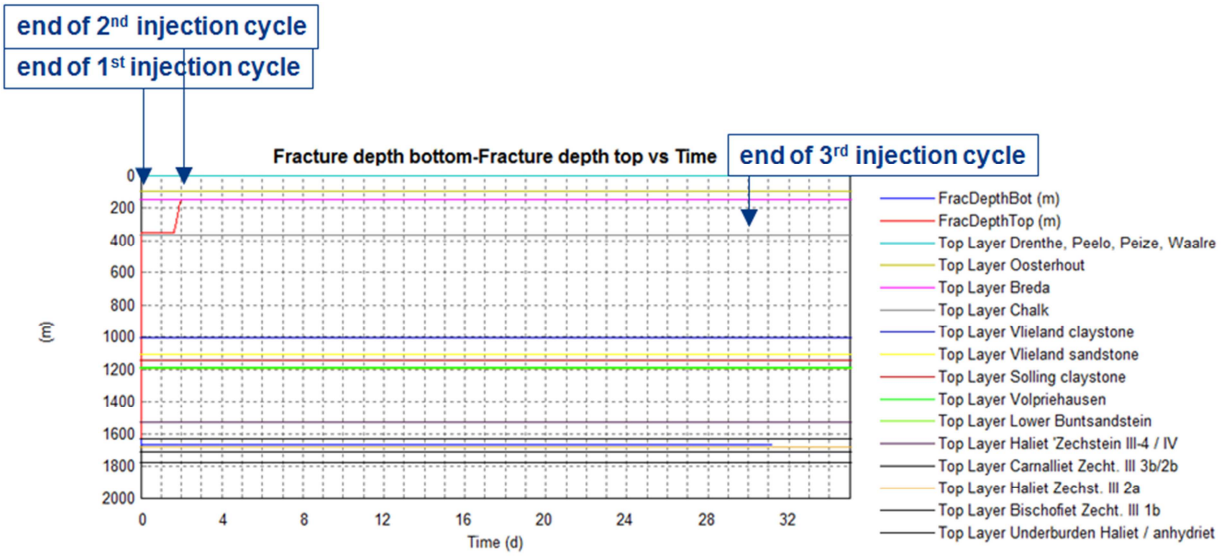

Figure 17b. Results after one month of injection of simulations using WI/CRI model. Low permeability of Vlieland sandstone (30 mD).

The fact that the Vlieland sandstone permeability 'had to be lowered' by a significant amount in order to have a clear impact on fracture growth can be explained by the fact that also a non-negligible amount of leakage takes place in the Bunter, chalk and Volpriehausen. This is confirmed by the next sensitivity, where the permeability of all permeable formations was lowered simultaneously by a factor 3 (sensitivity 9).

The result is shown in figure 18 below.

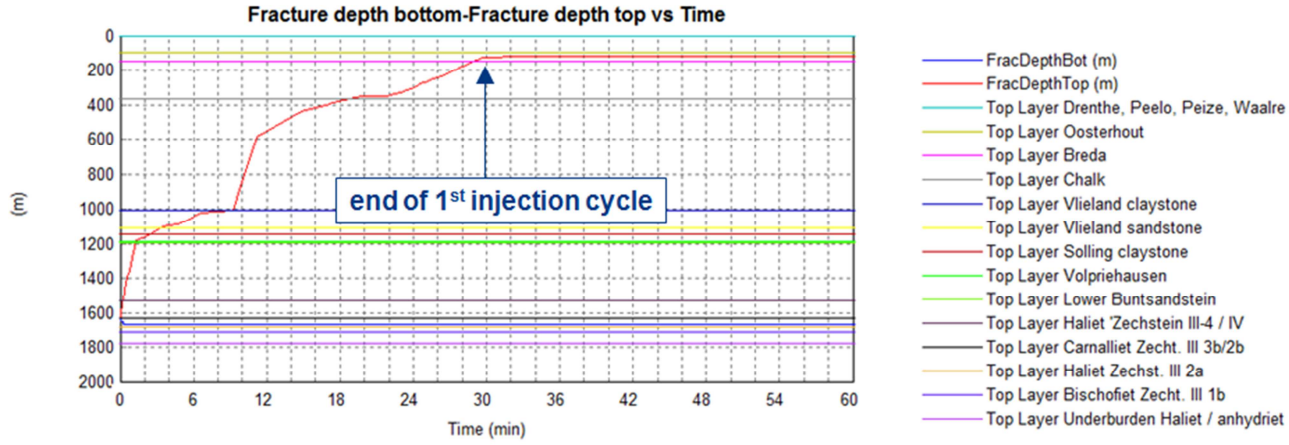

Figure 18. Results after 60 minutes of injection of simulations using WI/CRI model. For this case, all formations into which (some) brine leakage takes place had their permeabilities lowered by a factor 3.

As can be seen from figure 18, lowering the permeabilities of all leak-off formations by a factor 3 simultaneously results in a larger fracture. But lowering the permeability of only one of these formations by a factor 3 does not have a significant impact.

5.6 Further sensitivities

Also the following sensitivities were investigated. See appendix C for further details.

- Injection point (sensitivity. no 2): Injection from the top Halite instead of the top Carnalite does not impact the final results.
- Length of initial fracture (sensitivities no 11,12): In the WI/CRI injection model, the fracture length exhibits a limited increase beyond its initial value. This is a consequence of the assumed fracture shape (two half-ellipses). Therefore, for the initial fracture lengths of 100 m and 50 m, which are both lower than the base case, the final fracture upward height is larger. This is because the total leakage area has to remain approximately the same. Please note: as was discussed above, although most brine leaks away in the Vlieland sandstone, the leakage volumes in the low-k*h formations (Chalk, Volpriehausen, Bunter) are certainly non-negligible.

6. Conclusions

- A fracture propagation study was carried out in order to improve understanding of what happened during the leakage incident on 20 April 2018.
- In this study two different hydraulic fracture simulators were used that complement each other.
- The Leakage incident was modelled by three subsequent injection cycles:
    - Very high rate (50000 m3/h) during 30 minutes
    - High rate (1050 m3/h) during 47,5 hours
    - 'Medium' rate (100 m3/h) during 30 days
- Observed trends in injection pressure can be reasonably well reproduced by the simulations.
- The simulation study shows that during the first cycle with very high injection rate, a large fracture was created. This fracture propagated up toward the Vlieland sand/clay and Chalk, and possibly further upward towards the shallow high-permeability sands (Drente, Peelo, Peize, Waalre, Oosterhout), depending on the magnitude of the (unknown) stress contrasts between Vlieland sands and clays.
- The simulations also show that further upward fracture propagation during subsequent cycles of lower injection rate is unlikely.
- It is estimated that during the leakage incident on 20 April 2018 and the following month, about 150000 m3 of brine leaked away into the subsurface.
- About 90% of this volume is estimated to have leaked away into the Vlieland sandstone, whilst the other 10% has leaked away into the Chalk, Volpriehausen and lower Bunter.
- Formation pressure transient calculations show that pressure penetration fronts after about 1 year do not reach beyond 10 km into the Vlieland sandstone and not beyond 1 km in the other formations into which brine is leaking away.
- The Vlieland sandstone in the Veendam area is laterally continuous and very extensive with the same thickness over large distances. There are some fault networks, but these are not continuous. Therefore, no no-flow boundaries can be identified in this formation. Consequently, the leakage is not expected to result in laterally extensive areas of very high pore pressure which would be a requirement for possible earthquakes.

7. Epilogue (October 2018)

The fracture propagation study reported in this memo was carried out during May and June 2018, during a period that low-rate leakage was still ongoing. Meanwhile, based on the behaviour of the cavern cluster and on subsidence measurements, it was concluded that the leakage came to a halt significantly quicker than assumed initially.

In the original study, the following leakage rates were estimated (see paragraph 4.4):

- First month: 50000 m^3/h for 30 minutes, followed by 1050 m^3/h for 47.5 hours, followed by 100 m^3/h for 30 days.
- Second month and thereafter: 50 m^3/h.

According to the latest insights, these estimates are too conservative. Instead, it is now (still conservatively) estimated that the leakage rates were as follows:

- First month: 50000 m^3/h for 30 minutes, followed by 1050 m^3/h for 47.5 hours, followed by 100 m^3/h for 10 days.
- Second month and thereafter: zero.

Based on these revised cumulative injected volumes, estimates of brine penetration into the formations adjacent to TR-2 have been made. Results are shown in the table below.

Formation	**Brine volume leaked away (m^3)**	**Brine penetration front (m)**
Chalk	4000	0,38
Vlieland sandstone	90000	27
Volpriehausen	3000	4,5
Lower Bunter	3000	0,18
Total	~ 100000	

From this table, it can be seen that the final extent of brine penetrations in all formations is small. In particular, based on the latest insights, penetration in the Vlieland has reached a final maximum of 27 m, whereas in the previous estimates (see 4.4) it was forecasted to (possibly) extend over a few hundred metres within a couple of years.

An estimate of pore pressure penetration fronts at the end of the leakage period can be made using figures 7 (Vlieland) and 8 (Bunter). Assuming (again conservatively) that during the total leakage period of ~10 days the full pressure was present in the well, one can read off the corresponding pore pressure penetrations which are in between those for one day and one month. Thus, it is estimated that at the end of the leakage period, about 50% of the pressure had penetrated into the formation by some 500 m for the Vlieland and by some 100 m for the Bunter. Obviously, these pressure rises have equilibrated back to zero since the end of leakage.

References

1. G.Gheissary, P.A. Fokker, P.J.P. Egberts, F.J.T. Floris, G. Sommerauer and C.J. Kenter. Simulation of Fractures Induced by Produced Water Re-Injection in a Multi-Layer Reservoir. SPE 54735, presented at the SPE/ISRM Eurock '98 held in Trondheim, Norway, 8–10 July 1998.
2. P.J. van den Hoek. New 3D model for optimised design of hydraulic fractures and simulation of drill cuttings re-injection. SPE 26679, presented at SPE Offshore Europe, Aberdeen (1993).
3. Koning, E.J.L., Waterflooding under fracturing conditions, Ph.D. Thesis, Technical University of Delft, 1988.
4. Van den Hoek, P.J., Matsuura, T., De Kroon, M., and Gheissary, G.: "Simulation of Produced Water Injection Under Fracturing Conditions", SPE Prod. & Facilities 14 (3) August 1999, p. 166-176.
5. P.J. van den Hoek, G. Sommerauer, L. Nnabuihe, and D. Munro. Large-scale produced water re-injection under fracturing conditions in Oman. SPE 87267 (ADIPEC 0963), presented at Abu Dhabi Petr. Conference (2000).
6. P.J. van den Hoek, Z.I. Khatib, and G.J. Siemers. Causes of Injectivity Problems During Fractured Water Disposal and Their Remediation. SPE 74416, presented at SPE IPCEM, Villahermosa (2002).
7. M. Bai, S. Green, and P.J. van den Hoek. A parametric analysis of deep injection for waster disposal using a 3-D hydraulic fracture simulator (presented at NARMS conference, Toronto, 2002).
8. J.C. Noirot, P.J. van den Hoek, Dirk Zwarts, Hans Petter Bjoerndal, SPE, Rik Drenth, R. Al Masfry, B. Wassing, J. Saeby, M. Masoori, and A. Zarafi. Water Injection and Water Flooding Under Fracturing Conditions. SPE 81462, presented at SPE MEOS, Bahrain (2003).
9. S. Sathyamoorthy, P. Priyandoko, K.B. Flatval, A. Bulang, P.J. van den Hoek, and Y. Qiu. Radical Approach to Water Injection Scheme for Barton. SPE 84885, presented at SPE improved oil recovery conference in Asia Pacific, Kuala Lumpur (2003).
10. K.I. Ojukwu and P.J. van den Hoek. A New Way to Diagnose Injectivity Decline During Fractured Water Injection By Modifying Conventional Hall Analysis. SPE 89376, presented at SPE/DOE conference on improved oil recovery, Tulsa (2004).
11. B. Hustedt, Y. Qiu, D. Zwarts, and P.J. van den Hoek. Modeling Water-Injection Induced Fractures in Reservoir Simulation. SPE 95726, presented at SPE ATCE, Dallas (2005).
12. J. Sæby, H.P. Bjørndal, and P.J. van den Hoek. Managed Induced Fracturing Improves Waterflood Performance in South Oman. IPTC-10843, presented at IPTC, Doha (2005).
13. Hustedt, B., Qiu, Y., Zwarts, D., van Schijndel, L., and P.J. van den Hoek. The Impact of Water-Injection Induced Fractures on Reservoir Flow Dynamics: First Applications of a New Simulation Strategy. IPTC-10689, presented at IPTC, Doha (2005).
14. P.J. van den Hoek, B. Hustedt, M. Sobera, H. Mahani, R.A. Masfry, J. Snippe and D. Zwarts. Dynamic Induced Fractures in Waterfloods and EOR, SPE 115204, presented at the 2008 SPE Russian Oil & Gas Technical Conference and Exhibition held in Moscow, Russia, 28–30 October 2008.
15. B. Hustedt, D. Zwarts, H.-P. Bjoerndal, R. Masfry, and P.J. van den Hoek. Induced Fracturing in Reservoir Simulations: Application of a New Coupled Simulator to Waterflooding Field Examples. SPE Reservoir Evaluation & Engineering Journal, Vol. 11 (June 2008), p. 569-576.

16. A. Aniskin, I. Chmuzh, R. Sakhibgareev. Waterflood induced fracturing in the West Salym field. SPE 136560, presented at the 210 SPE Russian Oil & Gas Technical Conference and Exhibition held in Moscow, Russia, 26-28 October 2010.

17. Van den Hoek, P.J., Al-Masfry, R., Zwarts,D., Jansen, J.D., Hustedt,B., and Van Schijndel, L. Waterflooding Under Dynamic Induced Fractures: Reservoir Management and Optimization of Fractured Waterfloods. SPE Reservoir Evaluation & Engineering Journal, October 2009, p.671-682.

18. M. Khodaverdian, T.G. Sorop, P.J. van den Hoek, S.Sathyamoorthy and E. Okoh. Injectivity and fracturing in unconsolidated sand reservoirs: Waterflooding case study, offshore Nigeria. Paper Arma 10-139, prepared for presentation at the 44th US Rock mechanics Symposium and 5th US-Canada Rock mechanics Symposium, Salt Lake City, June 27-30, 2010.

19. M. Zwaan, R. Hartmans, S. Schoofs, B.R. de Zwart, G. Rocco, R. Adawi, F. Saadi, K. Shuaili, J. Lopez, J. Ita, T. L'Homme, T. Sorop, Y. Qiu, P.J. van den Hoek, F. Al-Kindy, S. Busaidi, and J. Fraser. EOR Field Management Through Well-Planned Surveillance. SPE 154620, presented at the SPE EOR Conference at Oil and Gas West Asia, Muscat, Oman, 16-18 April 2012.

20. A. Petrik and P.J. van den Hoek, Multi-zone Waterflood Top Seal Integrity Assurance: insights from advanced Pressure Fall Off analysis using Smart Well and DTS technologies offshore Sakhalin, Russia. SPE-181985, presented at the SPE Russian Petroleum Technology Conference and Exhibition held in Moscow, Russia, 24–26 October 2016.

21. Dougherty, R.L. & Abou-Sayed, A.S., Evaluation of the influence of in-situ reservoir conditions on the geometry of hydraulic fractures using a 3D simulator. SPE 13275 (1984).

22. Van den Hoek, P.J. Dimensions and Degree of Containment of Waterflood-Induced Fractures from Pressure Transient Analysis, SPERE, October 2005, 377-387.

23. Van Gent, H., Back, S., Urai, J., Kukla, P. and Reicherter, K. (2009). Paleostresses of the Groningen area, the Netherlands: Results of a seismic based structural reconstruction. Tectonophysics 470(1-2): 147-161.

Appendix A. Input data for base case.

Company name Nedmag

Well name TR2
Location Northern Netherlands
Date 20-04-2018
Description Nedmag TR2
Comments
Study to estimate fracture propagation as a result of brine leakage into the overburden layers above the top Zechstein III halite

INPUT

GEOLOGICAL MODEL

DepthTop (m)	LayerName
0	Drenthe, Peelo, Peize, Waalre
100	Oosterhout
150	Breda
368	Chalk
1010	Vlieland claystone
1110	Vlieland sandstone
1145	Solling claystone
1190	Volpriehausen
1197	Lower Buntsandstein
1530	Haliet 'Zechstein III-4 / IV
1630	Carnalliet Zecht. III 3b/2b
1680	Haliet Zechst. III 2a
1710	Bischofiet Zecht. III 1b
1780	Underburden Haliet / anhydriet

DepthTop (m)	DepthBottom (m)	LayerHeight (m)	StressTop (MPa)	StressBottom (MPa)	StressGrad (kPa/m)
0	100	100	0	1.58	15.8
100	150	50	1.58	2.37	15.8
150	368	218	2.37	5.814	15.8
368	1010	642	5.814	15.96	15.8
1010	1110	100	18.	19.58	15.8
1110	1145	35	17.54	18.09	15.8
1145	1190	45	19.36	20.07	15.8
1190	1197	7	18.8	18.91	15.8
1197	1530	333	18.91	24.17	15.8
1530	1630	100	28.11	29.69	15.8
1630	1680	50	29.95	30.74	15.8
1680	1710	30	30.87	31.34	15.8
1710	1780	70	31.42	32.53	15.8
1780	1e+004	8220	32.71	162.6	15.8

FormPresTop (MPa)	FormPresBot (MPa)	FormPresGrad (kPa/m)
0	1.1	11
1.1	1.65	11
1.65	4.048	11
4.048	11.11	11
11.11	12.21	11
12.21	12.6	11
12.6	13.09	11
13.09	13.17	11
13.17	16.83	11
16.83	17.93	11
17.93	18.48	11
18.48	18.81	11
18.81	19.58	11
19.58	110	11

ROCK PROPERTIES

DepthTop (m)	Permeability (md)	Porosity (-)	YoungModulus (MPa)	PoissonRatio (-)	FracToughnes (MPa*SQRT(m))
0	1.2e+004	0.3	1000	0.25	5
100	6000	0.3	1000	0.25	5
150	0.1	0.05	1000	0.25	5
368	1	0.05	1000	0.25	5
1010	0.1	0.15	5000	0.35	5
1110	300	0.2	5000	0.25	5
1145	0.1	0.05	5000	0.3	5
1190	50	0.2	5000	0.25	5
1197	1	0.1	5000	0.25	5
1530	0.1	0.01	2.5e+004	0.5	5
1630	0.1	0.01	2.5e+004	0.5	5
1680	0.1	0.01	2.5e+004	0.5	5
1710	0.1	0.01	2.5e+004	0.5	5
1780	0.1	0.01	2.5e+004	0.5	5

FORMATION PARAMETERS

Poro-elastic constant	0 -
Thermo-elastic constant	0 kPa/°C
GeoThermal gradient	0.035 °C/m
Reservoir temperature	60 °C
Heat capacity of rock	2560 kJ/(m³*°C)
Connate water saturation	0 -
Residual oil saturation	0 -
Total reservoir compressibility	5e-007 1/kPa
Formation fluid viscosity	0.5 mPa*s
Endpoint rel. perm. of oil	1 -
Endpoint rel. perm. of water	1 -

INJECTION FLUID & FILTER CAKE

Inj. water viscosity at inj. temp.	3.1 mPa*s
Inj. water viscosity at res. temp.	1 mPa*s
Inj. water heat capacity	4000 kJ/(m³*°C)
Inj. water density	1.3 g/cm³
Damage factor	0.1 -
Permeability	0.0001 md

FRACTURE DIMENSIONS

Init. fracture height upwards	0.5 m
Init. fracture height downwards	0.5 m
Init. fracture depth (TV)	1635 m
Init. fracture length	150 m
Drainage radius	1e+004 m

WELLBORE HYDRAULICS

S# Description (-)(-)	DepthBotAH (m)	DepthBotTV (m)	SectLengthAH (m)	SectLengthTV (m)
0 0	0	0	0	0
1 ? tubing	1650	1650	1650	1650

S# Description (-)(-)	DepthBotAH (m)	InnerDiam (mm)	OuterDiam (mm)	FrictionMult (-)
0 0	0	0	0	1
1 ? tubing	1650	0	2e+004	1

Init. fracture depth (AH) 1650 m

INJECTION CYCLES

InjTime (min)	InjDuration (mon)	InjRate (m³/day)	SolidsLoadng (vol ppm)	OilLoading (vol ppm)	InjWatSurfT (°C)
0	0.0006845	1.2e+006	0.001	0	59
30	0.06503	2.52e+004	0.001	0	59
2880	0.9856	2400	0.001	0	59